

Focusing of weak shock waves and the von Neumann paradox of oblique shock reflection

Esteban G. Tabak

Program in Applied and Computational Mathematics, Princeton University, Princeton, New Jersey 08544

Rodolfo R. Rosales

Department of Mathematics, Massachusetts Institute of Technology, Cambridge, Massachusetts 02139

(Received 18 June 1993; accepted 22 December 1993)

Some phenomena involving intersection of weak shock waves at small angles are considered: the focusing of curved fronts at arêtes, the transition between regular and irregular reflection of oblique shock waves on rigid walls and the diffraction patterns arising behind obstacles. The intersection of three shock waves plays a central role in most of these phenomena, giving rise to the von Neumann paradox of oblique shock reflection and to the curious transition between linear and fully nonlinear focusing investigated experimentally by Sturtevant and Kulkarny [J. Fluid Mech. **73**, 651 (1976)]. This "triple-point paradox" is studied in the context of an asymptotic model, and a solution is proposed that involves an unusual kind of singularity.

I. INTRODUCTION

Wave motion can often be modeled as an essentially one-dimensional phenomenon. Wave fronts may certainly be curved, but, in many situations, they still behave as if locally planar with curvature playing only a secondary role. This local one-dimensionality is a clue to much of our theoretical understanding of waves. Geometrical optics, for instance, treats high-frequency waves as if they had definite directions of propagation given by "rays." Nonlinear hyperbolic systems and shock waves are also best understood in nearly one-dimensional situations, where simple analytical models like the inviscid Burgers' equation or the Riemann problem and relatively simple experimental setups, such as shock-tubes, are often available.

There are many situations, however, in which these one-dimensional models are insufficient. The best known example is the diffraction of light through a crystal or after hitting an obstacle, where the failure of ray theory gave rise to the discovery of the wave-like character of light and, in a broader context, to quantum physics. Another is the intersection of two or more fronts, particularly for nonlinear waves. This includes phenomena arising in shock wave crossings, a shock's passage through the interface between two media and its reflection on a rigid wall. Yet another example is the focusing of concave fronts, where transverse effects destroy the nearly one-dimensional picture prior to focusing. All these situations abound in open problems and give rise to apparently paradoxical behaviors.

In this work, we concentrate on interactions involving almost parallel, weak shock waves. We have in mind two related problems: the focusing of a concave front and the reflection of nearly glancing weak shocks on rigid walls. A third problem, somewhat simpler but also intimately related to the previous two, is the diffraction of shock waves across singular rays, the "shadow lines" of geometrical optics. The reasons for the choice of this particular class of interactions are twofold: on the one hand, it includes many intriguing phenomena; on the other, a multiple scale modification of weakly nonlinear geometrical acoustics pro-

vides a unifying framework for its study. We will show that, in this asymptotic framework, the following paradox occurs: triple shocks, which the equations do not seem to admit, do nonetheless arise. In the context of oblique shock reflection, this is the core of the von Neumann paradox. We deal only with inviscid flows; the paradox cannot be resolved by invoking viscosity, unless one is willing to admit that the inviscid equations do not have a solution.

The tone of this paper will be mostly descriptive: many results will be stated without proof and, although numerical solutions will be freely displayed to illustrate phenomena and even to make points, the algorithm itself will not be explained in detail. Besides, we will concentrate more in posing paradoxes than in solving them. The main reference for missing details is Ref. 1. The numerical algorithm will be discussed in Ref. 2 and the analytic results in Refs. 3 and 4, where we will hopefully solve some of the questions opened here.

Over the years, problems of focusing and diffraction have captured the interest of physicists and mathematicians. Their solution, within the framework of linear geometrical optics, was found by R. N. Buchal and J. B. Keller in 1960,⁵ and made uniform by D. Ludwig in 1966.⁶ The transition between linear and nonlinear behavior was studied experimentally by B. Sturtevant and V. A. Kulkarny in 1976;⁷ their surprising results (summarized in Sec. II A) constitute one of the main motivations for the present work.

A thorough study of oblique shock reflection on rigid walls was carried out by J. von Neumann and a group of experimentalists at Princeton in 1943.^{8,9} Besides distinguishing the different types of reflection and explaining many of these in a completely satisfactory manner, von Neumann pointed out a variety of situations in which the theory was not at all clear and sometimes seemed to contradict the experiments. One of these situations, involving weak shocks at almost glancing incidence, gave rise to the "von Neumann paradox," which is the other main moti-

vation for the work which follows. Later work on this paradox can be found in Refs. 10–16.

The theory of weakly nonlinear geometrical acoustics, particularly for complex interactions, was developed in the seventies and eighties mainly by Y. Choquet-Bruhat, J. K. Hunter, J. B. Keller, A. Majda, and R. R. Rosales (see Ref. 17 for a review). Nonlinear expansions were conjectured at singular rays, caustics, and arêtes, based on the geometry of the linear solutions, in Refs. 18–20. In the present work we study the output of these expansions, which coincides with the equations of time dependent small disturbance transonic flow, and show that they predict the von Neumann paradox and the behavior at focusing of weak shock waves.

This paper is structured as follows. In Sec. II, we describe the experiments that motivated this work and make some physical connections between them. In Sec. III, we introduce the asymptotic model, show how it applies to the different phenomena under study, and discuss some important symmetries and exact solutions. In Sec. IV, we show the “triple shock paradox” arising in oblique shock reflection, focusing of curved fronts, and a class of modified singular rays. Finally, in Sec. V, we explain the need of singular behavior behind the triple point, verify this insight numerically, and briefly discuss some of its consequences.

II. SOME PUZZLES INVOLVING WEAK SHOCK WAVES

In this section, we describe some simple yet intriguing phenomena involving weak shock waves moving into a gas at rest and intersecting at small angles. Understanding these phenomena is required to complete the theory of weakly nonlinear geometrical acoustics.

A. Focusing of weak shock waves

The focusing of curved fronts is a process extraordinarily rich in qualitatively different behaviors yielding patterns not yet completely understood. Even linear theory is far from trivial, and the weakest nonlinearity gives rise to apparent paradoxes. Solving these paradoxes is crucial to complete the insight provided by geometrical acoustics, that describes the local behavior of the fronts away from the focus. The problem has also practical interest, since most wave fronts arising in nature are curved, so focusing is almost as ubiquitous as the waves themselves. For a first glimpse of this variety of behaviors, let us briefly describe the linear and fully nonlinear cases.

Linear focusing (Fig. 1) is best described in the language of geometrical acoustics. The fronts move normal to themselves at the velocity of sound. Introducing the bi-characteristics or “rays,” which are straight lines everywhere normal to the fronts, we can write an ordinary differential equation for the wave’s amplitude, which states that energy is conserved on ray tubes. These tubes, however, collapse at the envelopes of the rays, called caustics, yielding in principle an infinite value for the wave’s amplitude. The first crossing of rays takes place at the “arête,” that evolves from the point of maximal curvature in the

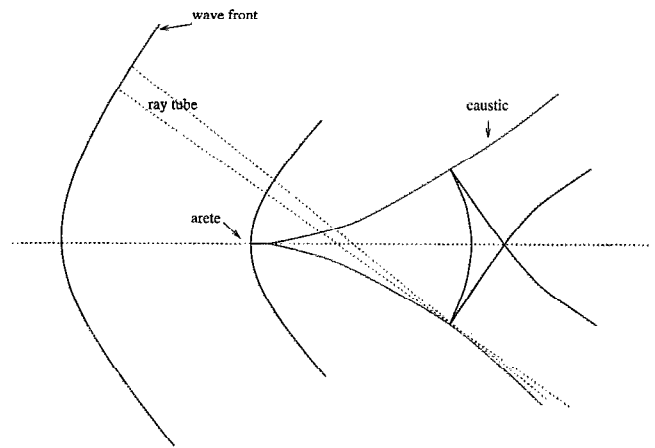


FIG. 1. Linear focusing. Ray tubes collapse at the caustics, which originate at the arête.

initial front. Thus the standard configuration, known as a swallow-tail, has two caustics meeting at an arête.

The situation in the fully nonlinear case (Fig. 2) is completely different. As a section of the focusing front approaches the arête, its amplitude’s growth locally accelerates the front, flattening it up, and avoiding the ray crossing and front folding altogether. Instead, the high pressure behind the arête, after pushing the front ahead, diffracts through compression waves, which eventually become shocks. Triple points therefore arise at the intersection between these diffracted shocks and the focusing wave; and then move away from the focusing region. An approximate theoretical description of this process is provided by Whitham’s Geometrical Shock Dynamics.²¹

Sturtevant and Kulkarny⁷ performed a series of carefully designed experiments to study the transition between the linear and nonlinear regimes. They created plane waves

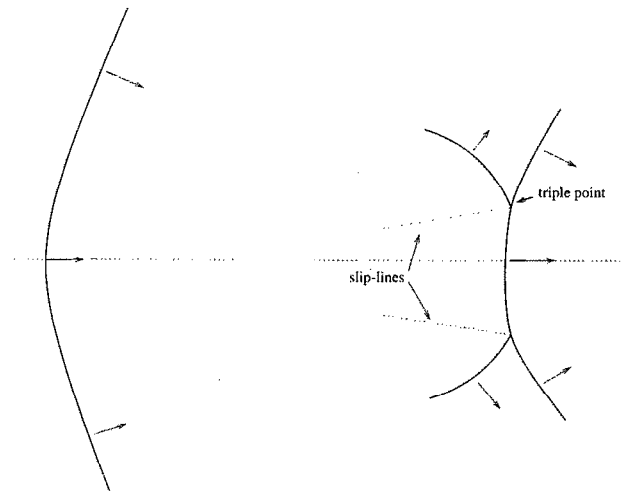


FIG. 2. Fully nonlinear focusing. The amplification of intensity as the front approaches the arête leads to a local acceleration of the front, which makes it flatten up, avoiding focusing altogether. The high pressure behind the failed arête diffracts to the sides through compressive waves, which eventually break into shocks. Thus triple points form along the focusing front, and then move away from the focusing region.

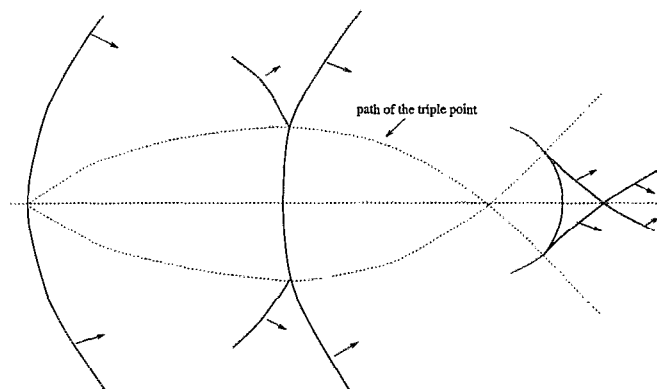


FIG. 3. Focusing at an intermediate amplitude. The nonlinear flattening with formation of diffracted shocks always takes place. If the shocks are weak enough, the triple points eventually collide at the axis of symmetry, yielding a configuration qualitatively similar to the linear swallow-tail.

of different amplitudes in a shock-tube, and made them reflect on a curved mirror at the end of the tube, to produce curved focusing shocks of a controlled initial wave-front shape. They found for strong shocks the configuration of Fig. 2. For weaker shocks (Fig. 3), nonlinearity still prevails at the beginning, giving rise to two diverging triple points. These, however, eventually converge and cross, creating a pattern visually equivalent to the linear swallow-tail. This process takes place even for vanishingly small amplitudes, yielding the surprising result that the linear configuration is always preceded by a transient nonlinear

one. In the linear limit, the duration of the nonlinear transient state tends to zero and the path of the triple shocks shrinks to a point.

B. Oblique shock reflection on a rigid wall

Another phenomenon closely related to nonlinear focusing is the reflection of a shock wave on a rigid wall. This was thoroughly studied by von Neumann in 1944^{8,9} both theoretically and experimentally. When a sufficiently weak shock wave hits a wedge, a pattern known as “regular reflection” arises. In this [Fig. 4(a)], the velocity normal to the wall is set back to zero by a reflected shock. For larger amplitudes, however, this pattern can be shown not to hold. Instead [Fig. 4(b)], the experiments give, for a wide range of parameters, a “Mach reflection,” in which the intersection between the incident and reflected shocks detaches from the wall, and a glancing, much stronger shock, the “Mach stem,” appears. Behind the point where the three shocks meet, a slip line marks the discontinuity in entropy between the gas that went through the incident and reflected shocks and the gas that crossed the Mach stem.

These two kinds of reflection do not fill the whole field of parameters. Particularly pertinent to our study is what happens to weak shock waves at almost glancing incidence. Figure 4(c) shows the boundary in angle-amplitude space below which regular reflection is not allowed. For small enough amplitudes, neither regular nor Mach reflection can take place below this line. The experiments performed

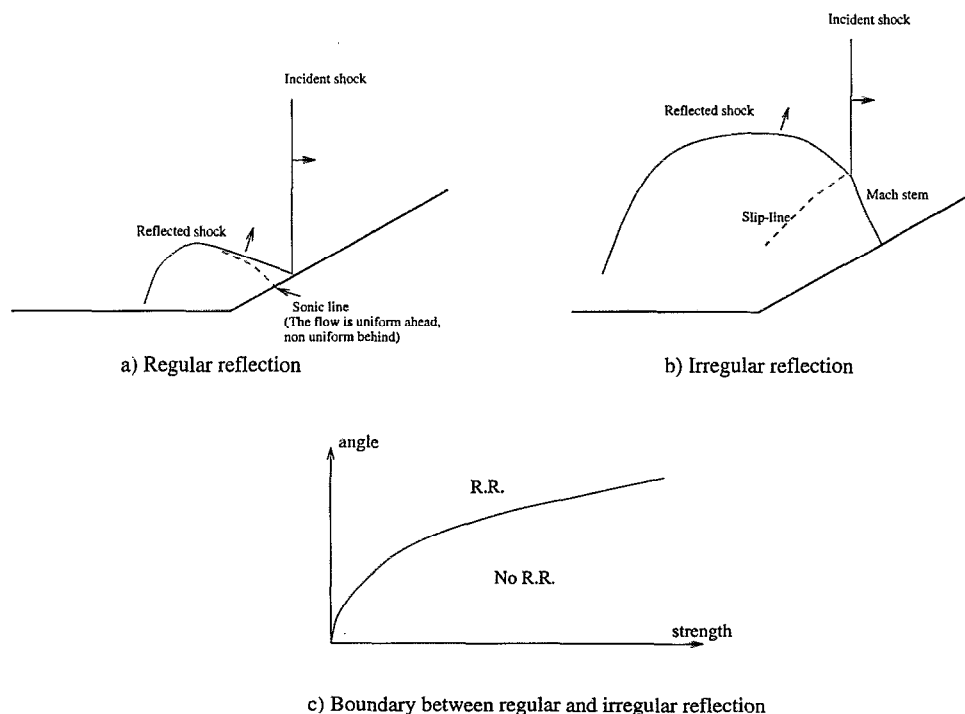


FIG. 4. Reflection patterns. When a shock moving glancing to a wall reaches a wedge, a great variety of configurations may occur. For large enough angles or small enough intensity of the shock, regular reflection takes place. For relatively small angles and strong shocks, a Mach-stem arises. The von Neumann paradox arises in situations when both the wedge-angle and the shock-intensity are small, and regular reflection is not allowed.

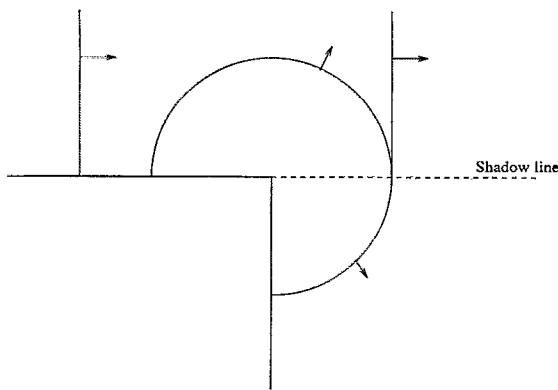


FIG. 5. Linear singular ray. Across the shadow line, diffraction processes occur, whereby the dark and illuminated regions learn of the presence of each other.

by von Neumann yielded nonetheless a configuration very much alike a Mach reflection, but with shocks that did not seem to satisfy the Rankine–Hugoniot jump conditions. This apparent contradiction is known as the “von Neumann paradox” of oblique shock reflection.

We can relate these phenomena to the focusing of shock waves by considering an axisymmetric front and replacing its axis of symmetry by a wall, an analogy perfectly correct if we neglect viscosity. If we do this conceptual change in Fig. 1, we see a curved shock wave reflecting on a wall; as it has zero amplitude, it gives rise to regular reflection. In Fig. 2, instead, we see a fully nonlinear case yielding a Mach stem. Finally, for weak waves, we find ourselves in the context of the von Neumann paradox. Observe that the arête corresponds to an incident shock with zero angle, hence nonlinear effects are to be expected even for negligibly small intensities. But the incident shock is curved; as a more oblique section approaches the wall, regular reflection is again allowed, and we get the delayed swallow-tail of Fig. 3. To predict whether a symmetric concave front will give rise to a swallow-tail or to a pattern of diverging triple shocks, it is enough to look at the parameters far away from the axis of symmetry, and check from Fig. 4(c) which kind of reflection the asymptotic slope and intensity of the shock would yield.

C. Singular rays

Another failure of geometrical acoustics occurs behind obstacles, along the so-called shadow lines, where diffraction effects neglected by the theory become important. Consider a shock wave moving parallel to a wall that ends abruptly at a corner (Fig. 5). After the wall’s end, ray theory predicts a discontinuity in behavior across a curve—the shadow line or singular ray—that continues the line of the wall. Above this, in the “illuminated” region of geometrical optics, the shock continues propagating at a uniform horizontal velocity; below, in the “shade,” the medium remains undisturbed. This discontinuous picture is contradicted both by experiments and analytic results. The solution to this problem in the linear case was found in Ref. 5. In a thin layer surrounding the shadow line, trans-

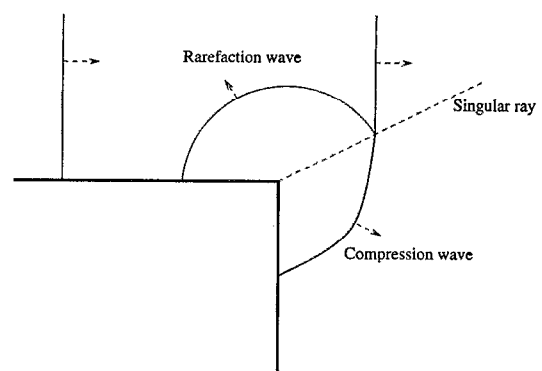


FIG. 6. Nonlinear singular ray. The shadow line goes up due to the higher velocity of sound in the more pressurized region.

verse effects become comparable to the longitudinal ones, henceforth affecting the balance of geometrical acoustics. The resulting picture can be best understood using Huyghens’ theory of light: the acute corner acts as a point source, emitting circular waves that darken the medium behind the shock and illuminate it below the shadow line.

In the nonlinear case, we should expect a similar behavior, only geometrically distorted by the nonuniformity of wave speeds. The singular ray moves up (Fig. 6), due to the faster propagation of sound waves in the upper region, where pressure is higher. The compression wave steepens up and forms a curved shock, that continues the straight remaining part of the original shock into the nonuniform diffractive region.

Singular rays have a much simpler structure than arêtes, caustics, and Mach-stems. We will see, however, that they are closely related to all three of them, so their simplicity might help understanding the “paradoxical” behavior of their more sophisticated relatives.

III. ASYMPTOTIC MODEL

In this section, we describe an asymptotic model for the behavior of weak shock waves at singular rays, arêtes, and almost glancing reflection on rigid walls. We motivate the model’s geometrical ansatz and display its equations, pose initial-value problems corresponding to the different phenomena, discuss some of their symmetries and show an important family of exact solutions.

A. The asymptotic equations

Our asymptotic model will use the equations of time dependent small disturbance transonic flow. We will not derive these equations here (for derivations see for instance Refs. 18–20), but we will briefly motivate their geometrical ansatz. The idea is basically an extension to weakly nonlinear situations of the geometrical diffraction theory developed in Ref. 5.

Weakly nonlinear geometrical acoustics considers fronts that are locally planar, with small wave amplitude [say $O(\epsilon)$] and short wavelengths of the same order in an appropriate nondimensionalization. The plane wave approximation reduces the number of independent variables

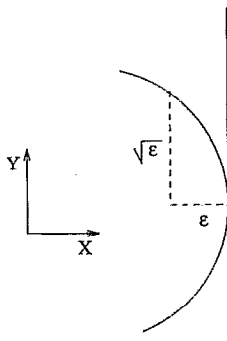


FIG. 7. Scaling for a singular ray. The same scale applies to the transition from regular to irregular reflection of weak shock waves and to weakly nonlinear arêtes.

to two (time and the direction of propagation) and the number of dependent variables to one. The amplitude is chosen at the threshold for nonlinear effects. These approximations fail close to singular rays, caustics, arêtes and, in general, locations where more than one front meet. To describe a linear singular ray, for instance, we need different scalings for the two spatial coordinates. If we consider a frame of reference moving at the velocity c of the straight front, and introduce a small parameter ϵ so as to magnify the vicinity of the singular ray, it is clear from Fig. 7 that, to the longitudinal variable $x = (X - cT)/\epsilon$, corresponds the “slower” transversal $y = Y/\epsilon^{1/2}$. This same scaling can be used for weakly nonlinear singular rays with an $O(\epsilon)$ amplitude.²⁰

The $(\epsilon, \epsilon^{1/2})$ scaling also applies to the transition from regular to irregular reflection in the context of the von Neumann paradox. This follows from the fact that, for small amplitudes, the cotangent of the angle below which regular reflection cannot hold scales as the square root of the shock’s strength [see Fig. 4(c)], which must be of the same order of the wavelength in the X direction for weakly nonlinear effects to apply.

The scales for a linear arête are different, since this involves a front with continuous slope but infinite curvature. It can be seen that the variables to adopt in this case are $(X - cT)/\epsilon$ and $Y/\epsilon^{3/4}$, which require an $O(\epsilon^{1/2})$ amplitude for nonlinear effects to manifest themselves. This seems to indicate (see Ref. 22 for a similar argument regarding caustics) that the arêtes of weakly nonlinear acoustics are always linear. The reasoning proceeds as follows: at a linear arête, the amplitude is $\epsilon^{-1/4}$ higher than at the outer solution. But this amplification factor falls short of the $\epsilon^{-1/2}$ which, multiplied by the $O(\epsilon)$ amplitude of the incoming focusing wave—as given by weakly nonlinear geometrical acoustics—would yield the $O(\epsilon^{1/2})$ threshold of nonlinearity. Nevertheless, the experiments of Sturtevant and Kulkarny and the arguments of Sec. I lead to the opposite conclusion, that nonlinear effects are always significant at an arête. Fortunately, they also show why the preceding argument fails: the infinite curvature of the linear geometry is never reached; before that, the smoother scaling of the previous paragraph, corresponding to a front

that has not yet focused, gives rise, in the context of the von Neumann paradox, to nonlinear diverging triple points. Therefore, nonlinearity manifests itself by altering the linear geometry, flattening the front and replacing the linear arête by a completely different configuration.

We see that the same scaling applies to singular rays, pseudo-Mach-stems and nonlinear arêtes. Doing the corresponding asymptotic expansion (see for instance Refs. 18 and 20) yields a set of equations whose canonical form is

$$\begin{aligned} \sigma_t + \left(\frac{\sigma^2}{2}\right)_x + \eta_y &= 0, \\ \sigma_y - \eta_x &= 0. \end{aligned} \quad (1)$$

Here σ is proportional to the $O(\epsilon)$ term in the perturbation to a constant state of density, pressure, temperature, and longitudinal velocity, while the transversal velocity begins at $O(\epsilon^{3/2})$, with a term proportional to η . These equations, which are the same as those of unsteady small disturbance transonic flow, constitute the basic tool of this work. Their associated jump conditions across a shock with position given implicitly by $S(x, y, t) = 0$ are

$$\begin{aligned} (S_t + S_x \bar{\sigma})[\sigma] + S_y[\eta] &= 0, \\ S_y[\sigma] - S_x[\eta] &= 0, \end{aligned}$$

where the brackets stand for jumps in the enclosed variables, and $\bar{\sigma}$ for the average of σ on the two sides of the shock. Equivalently we can write

$$\begin{aligned} S_t &= -\left(\frac{S_y^2}{S_x} + S_x \bar{\sigma}\right), \\ \frac{[\eta]}{[\sigma]} &= \frac{S_y}{S_x}. \end{aligned} \quad (2)$$

We can normalize S at any point to have $S_x = 1$ and $S_y = -\alpha$, where α is the cotangent of the shock’s inclination angle. Then, for straight shocks, we can rewrite Eqs. (2) as

$$\begin{aligned} x - \alpha y - (\bar{\sigma} + \alpha^2)t &= \text{const}, \\ [\eta] &= -\alpha[\sigma]. \end{aligned} \quad (3)$$

The entropy condition requires σ to decrease from left to right across shocks.

B. Model problems

We need to complement the equations in (1) with appropriate initial and boundary conditions for the different physical problems. Let us begin with oblique shock reflection. The condition at the wall is simply $\eta = 0$. The conditions at the time at which a glancing shock hits a wedge are plotted in Fig. 8(a). It seems intuitively obvious that the corresponding initial conditions for the model equations (1) are those represented in Fig. 8(b) (a detailed justification will be provided in Ref. 4). We have chosen to parametrize the angle of incidence of the shock by its cotangent α .

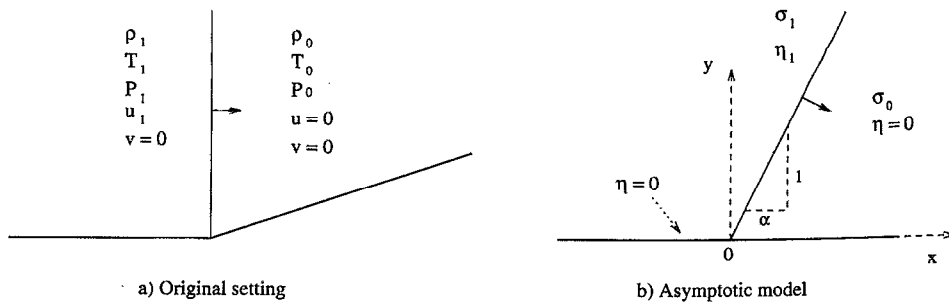


FIG. 8. Initial conditions for oblique shock reflection.

For a singular ray, there are no boundaries, and the conditions in both physical space and the asymptotic model immediately after a glancing shock has reached the end of an obstacle are plotted in Figs. 9(a) and 9(b). In Fig. 9(c), we have represented another initial condition, corresponding to what we will call a “modified” singular ray, whose relevance will be explained in Sec. IV.

The design of initial conditions for a focusing front involves a good deal of arbitrariness, since there is not a clear “time zero” for focusing as there was for shock reflection and singular rays. For our numerical computations, we have chosen the configuration of Fig. 10, with an initial front consisting of a quadratic parabola which, from some point on, continues as a straight line.

C. Symmetries; elliptic and hyperbolic domains

Both Eqs. (1) and the initial conditions for the different problems have a number of symmetries with important consequences. First, the equations’ invariance under the Galilean transformation

$$\begin{aligned} \sigma &\rightarrow \sigma + \sigma_0, \\ x &\rightarrow x - \sigma_0 t \end{aligned} \quad (4)$$

allows us to take $\sigma_0=0$ in all four problems. The invariance under

$$\begin{aligned} x &\rightarrow cx, \\ y &\rightarrow c^{1/2}y, \end{aligned}$$

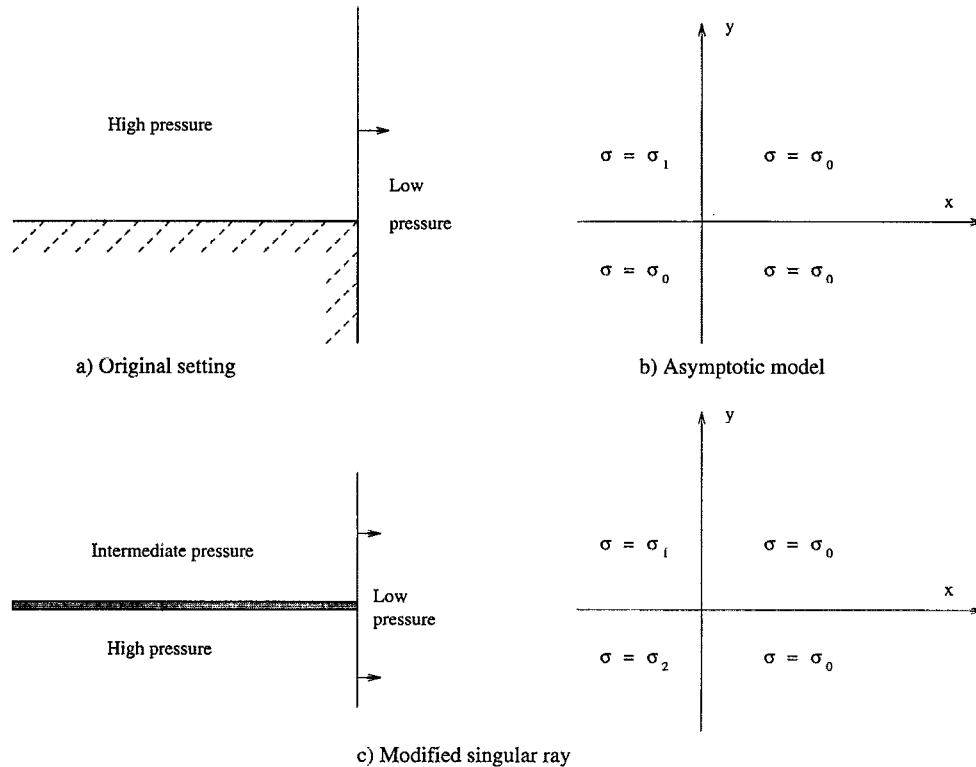


FIG. 9. Initial conditions for standard and modified singular rays.

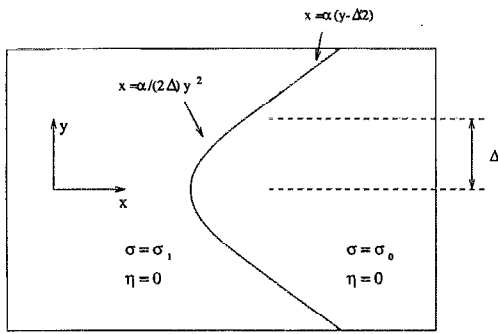


FIG. 10. Initial conditions for focusing.

$$\sigma \rightarrow c\sigma, \quad (5)$$

$$\eta \rightarrow c^{3/2}\eta$$

leaves σ_1/α^2 as the only parameter in the shock reflection problem, makes the choice of σ_1 arbitrary in standard singular rays, and reduces the choices, in modified singular rays, to that of the quotient σ_2/σ_1 and, in focusing, to that of a quotient between σ_1 and the curvature at the origin plus again a value of σ_1/α^2 , with α the slope of the straight part of the shock. Finally, the equations in (1) and the initial conditions for shock reflection and both standard and modified singular rays are invariant under the stretching

$$\begin{aligned} x &\rightarrow cx, \\ y &\rightarrow cy, \\ t &\rightarrow ct. \end{aligned} \quad (6)$$

This implies that, in these cases, the solution is a function of $\xi = x/t$ and $\tau = y/t$ alone. In these variables, the equations read

$$\begin{aligned} -\xi\sigma_\xi - \tau\sigma_\tau + (\sigma^2/2)_\xi + \eta_\tau &= 0, \\ \sigma_\tau - \eta_\xi &= 0. \end{aligned} \quad (7)$$

The reason for calling τ the quotient y/t is that, as we will see, it really acts as a time-like variable. In a way, the unsteady patterns travel away from the axis $\tau=0$, so their distances from it become a measure of the time elapsed. The characteristics of (7) are

$$d\xi/d\tau = -\tau/2 \pm \sqrt{\tau^2/4 + \xi - \bar{\sigma}}, \quad (8)$$

where $\bar{\sigma}$ stands for σ in smooth regions and for its average on the two sides of shocks [for shocks, $d\xi/d\tau$ in (8) is the shock speed in the (ξ, τ) coordinates]. The equations in (7) are hyperbolic for $\tau^2/4 + \xi - \bar{\sigma} > 0$ and elliptic elsewhere. There is a strong parallel between the appearance of elliptic and hyperbolic domains for (7) and that of subsonic and supersonic flows for both (1) and the original equations of gas dynamics. We will make this parallel precise in Refs. 3 and 4. An important related result is that, for waves propagating into a gas at rest, the solution can be locally non-constant only in the elliptic ("subsonic") domain.

D. A family of exact solutions

We will now compute the simple waves of (7), i.e., the solutions that depend on only one parameter. In regions where the solution is smooth, we can rewrite (7) as

$$\begin{aligned} -(\xi - \sigma)\sigma_\xi - \tau\sigma_\tau + \eta_\tau &= 0, \\ \sigma_\tau - \eta_\xi &= 0. \end{aligned}$$

This suggests switching to the semi-implicit coordinates $\chi = \xi - \sigma$, τ . In these, the equations become

$$\begin{aligned} -\chi\sigma_\chi - \tau\sigma_\tau + \eta_\tau + \frac{\partial(\sigma, \eta)}{\partial(\chi, \tau)} &= 0, \\ \sigma_\tau - \eta_\chi &= 0, \end{aligned} \quad (9)$$

where $\partial(\sigma, \eta)/\partial(\chi, \tau)$ is the Jacobian $\sigma_\chi\eta_\tau - \sigma_\tau\eta_\chi$. Notice that these equations are almost the same as (7), with the Jacobian replacing the nonlinear term $(\sigma^2/2)_\xi$. But the Jacobian will vanish whenever σ and η are functionally dependent, so this formulation is particularly suitable to the study of simple waves, where both σ and η are functions of the same variable S . Assume $\sigma = F(S)$ and $\eta = G(S)$. Then (9) becomes

$$\begin{aligned} (-\chi S_\chi - \tau S_\tau)F'(S) + S_\tau G'(S) &= 0, \\ S_\tau F'(S) - S_\chi G'(S) &= 0. \end{aligned}$$

For this system to have nontrivial solutions, we must have

$$S_\tau/S_\chi = \tau/2 \pm \sqrt{\tau^2/4 + \chi}$$

which can be read as an ordinary differential equation for the contour lines of S :

$$\frac{d\chi}{d\tau} = -\tau/2 \mp \sqrt{\tau^2/4 + \chi}. \quad (10)$$

This equation has the one-parameter family of solutions $\chi = \alpha\tau + \alpha^2$, together with its envelope $\chi = -\tau^2/4$, which coincides with the boundary of the elliptic region. These contour lines, which we will call "pseudocharacteristics," are plotted in Fig. 11.

Notice that, at a given point (χ, τ) , α can be computed as $\alpha = -\tau/2 \mp \sqrt{\tau^2/4 + \chi}$. But there is a one to one relation between α and the contour lines of S , so in particular we can take $S = \alpha$. Then we have found the following families of solutions, depending on an arbitrary function F and the sign chosen for the square root: $\sigma = F(S)$, $\eta = G(S)$, with $S = -\tau/2 \mp \sqrt{\tau^2/4 + \chi}$ and $G'(S) = -SF'(S)$. The pseudocharacteristics on which we build these solutions are indeed characteristics, because the only difference between (8) and (10) is the term $d\sigma/d\tau = d\xi/d\tau - d\chi/d\tau$, and this vanishes along a pseudocharacteristic, where σ is constant by construction.

These solutions hold in the hyperbolic domain $\tau^2 + 4\chi > 0$. But the method also works, at least formally, in the elliptic domain, yielding complex results. This is not a problem in the linear case, where real and imaginary parts decouple and we can keep either as a real solution (notice that, in this linear case, $\xi = \chi$). This suggests a simple recipe for solving the linear equations with data given on the

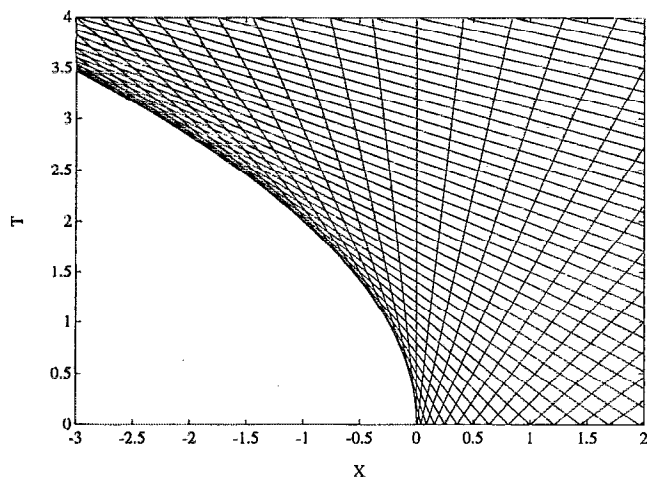


FIG. 11. Pseudocharacteristics in the implicit coordinates χ , τ . Both families of characteristics are tangent to the parabolic line.

boundary of the elliptic domain: Consider these data as the imaginary part of a complex function $F(S)$ [or $G(S)$ if η is given instead of σ] that we only need to extend analytically into the interior of the elliptic domain to get the full solution. In other words, we have found that, in the system of coordinates $(\tau/2, \sqrt{-\tau^2/4 - \chi})$, the linear equations imply Laplace's for both σ and η . We will use this procedure in the following section to compute the exact linear solutions for unsteady regular reflection and singular rays.

There is a more explicit representation of the simple waves in the hyperbolic domain. Notice that, since σ is constant along pseudocharacteristics, these are straight lines in both the implicit coordinates (χ, τ) and the explicit (ξ, τ) . This suggests considering any one-parameter family of straight lines in the (ξ, τ) plane and look for a solution to (7) where both σ and η have these as contour lines. We will show next that such a solution, necessarily a simple wave, always exist, and has a very simple explicit formula. For this, consider the family as generated by its envelope, given parametrically by $\xi = \xi_0(\theta)$, $\tau = \tau_0(\theta)$. Here θ is the angle of the tangent to the curve, so we must have $\tau'_0(\theta) = \tan(\theta)\xi'_0(\theta)$. Notice that this will be trivially satisfied if $\tau'_0(\theta) = \xi'_0(\theta) = 0$, so we can consider a single point as a particular case of enveloping curve. Now, in the region towards which $(\xi_0(\theta), \tau_0(\theta))$ is concave, we introduce a system of coordinates $(\theta(\xi, \tau), \psi(\xi, \tau))$ in the following way (Fig. 12): we trace from (ξ, τ) a tangent to $(\xi_0(\theta), \tau_0(\theta))$, and denote by θ the angle of inclination of this tangent and by ψ the distance along it from the curve. Then

$$\theta = \tan^{-1} \left(\frac{\tau - \tau_0(\theta)}{\xi - \xi_0(\theta)} \right),$$

$$\psi = \frac{\xi - \xi_0(\theta)}{\cos(\theta)}.$$

The equations in (7) become, after some manipulation, if we consider the case in which σ and η are functions of θ alone,

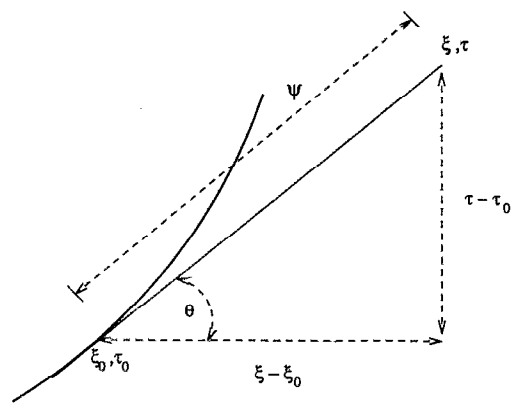


FIG. 12. New coordinates, appropriate for an explicit description of the simple waves.

$$(\cos\theta)\sigma_\theta + (\sin\theta)\eta_\theta = 0,$$

$$\left[(\xi_0(\theta) - \sigma) \frac{\tau_0(\theta)}{\tan(\theta)} - \frac{1}{\tan^2(\theta)} \right] \sigma_\theta = 0.$$

Hence either $\sigma_\theta = 0$ or

$$\sigma = \xi_0(\theta) - \frac{\tau_0(\theta)}{\tan(\theta)} - \frac{1}{\tan^2(\theta)} \quad (11)$$

with η defined by the first formula. This is an explicit formula for our simple waves. Notice that the arbitrary choice of $F(S)$ in the implicit formulation corresponds to that of the family's envelope in the explicit coordinates. In particular, the solution with $\xi_0(\theta)$ and $\tau_0(\theta)$ constant (a fan emanating from a point) is

$$\sigma = \xi_0 - \tau_0 \frac{\xi - \xi_0}{\tau - \tau_0} - \left(\frac{\xi - \xi_0}{\tau - \tau_0} \right)^2,$$

$$\eta = c + \frac{\tau_0}{2} \left(\frac{\xi - \xi_0}{\tau - \tau_0} \right)^2 + \frac{2}{3} \left(\frac{\xi - \xi_0}{\tau - \tau_0} \right)^3. \quad (12)$$

Just as the implicit formulation could be used in the elliptic domain, so can the explicit formulas be applied in the region not covered by rays, i.e., the region towards which the envelope is convex. There θ and the solution (11) are complex. This again is not a problem in the linear case, where real and imaginary parts decouple, and either part yields an exact solution.

E. A numerical algorithm

In the following sections, we will often use numerical results to illustrate phenomena and motivate discussions. The algorithm that we use will be fully described in Ref. 2; a very brief description here seems appropriate though to make this paper self-contained.

Our goal is to solve Eqs. (1) numerically for different initial and boundary conditions. The fact that makes this a delicate task is that the planes with constant time are characteristic surfaces of the equations. Advancing a solution in time is therefore a nonlocal operation; certain perturbations propagate with infinite velocity. In the presence of

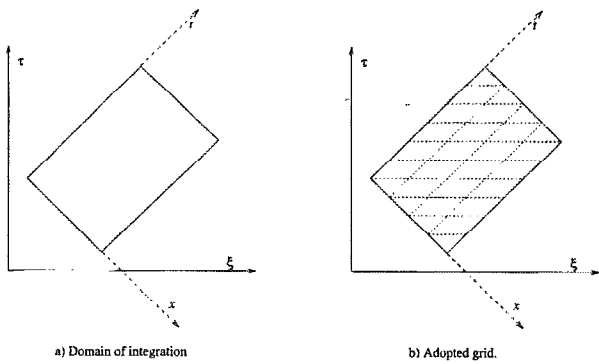


FIG. 13. "Oblique" coordinates for the numerical solution of the asymptotic equations.

shocks, this leads to spurious dispersive effects that ruin the accuracy of any standard numerical method.

A remedy that we have found to this is to switch to the "oblique," noncharacteristic coordinates $\xi = t + x$, $\tau = t - x$, y . In these coordinates, the equations are

$$(\sigma - \sigma^2/2)_\tau + (\sigma + \sigma^2/2)_\xi + \eta_y = 0,$$

$$\eta_\tau - \eta_\xi + \sigma_y = 0.$$

Introducing $\omega = \sigma - \sigma^2/2$, with inverse $\sigma = 1 - \sqrt{1 - 2\omega}$ (assuming $\sigma < 1$ and $\omega < 1/2$), we get

$$\omega_\tau - (\omega + 2\sqrt{1 - \omega})_\xi + \eta_y = 0,$$

$$\eta_\tau - \eta_\xi - (\sqrt{1 - 2\omega})_y = 0.$$

Here τ is not a characteristic of the equations; indeed, it is a valid time-like variable. Thus we advance in τ instead of t , using a fractional-step alternate-direction procedure to decouple the ξ and y derivatives. The two systems to solve are

$$\begin{aligned} \omega_\tau - (\omega + 2\sqrt{1 - \omega})_\xi &= 0, \\ \eta_\tau - \eta_\xi &= 0, \end{aligned}$$

and

$$\begin{aligned} \omega_\tau + \eta_y &= 0, \\ \eta_\tau - (\sqrt{1 - 2\omega})_y &= 0. \end{aligned}$$

The first system decouples into two scalar equations, while the second may be viewed as describing a polytropic evolution of gas dynamics in Lagrangian coordinates, with ω acting as specific volume, $(-\eta)$ as velocity, and with pressure given by the convex $P(\omega) = \sqrt{1 - 2\omega}$. We solve both systems with a second order Godunov method that works on nonrectangular grids,²³ since in the new coordinates (ξ, y, τ) the domain of integration for fixed y has the shape sketched in Fig. 13, which cannot be covered by a rectangular mesh. The boundary conditions that complement this algorithm will be discussed in Ref. 2.

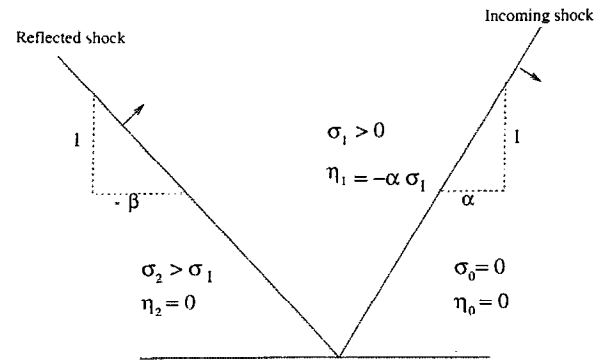


FIG. 14. Steady regular reflection. The equations for the reflected shock have two solutions for $\sigma_1/\alpha^2 < 1/2$ and none otherwise. To decide which solution really takes place, the unsteady process has to be considered.

IV. THE VON NEUMANN PARADOX IN THE ASYMPTOTIC MODEL

In this section, we show evidence that triple shocks, which the equations in principle do not admit, do nonetheless occur in many situations. We discuss regular reflection, both steady and unsteady, and show that this can only take place for a limited range of parameters. This fact and the theorem that we prove next on triple shocks not being allowed constitute the core of the von Neumann paradox. This gets enhanced when we show, in a half-theoretical, half-experimental way, that triple shocks need to arise, at least for a range of parameters, in unsteady irregular reflection. We find the same paradox in a class of modified singular rays, where we can prove rigorously that triple shocks occur. Finally, we show numerically that triple shocks arise in both weak and strong focusing of curved fronts, occurring in the latter as in shock reflection, and in the former as an inverted triple shock that replaces the linear caustic.

A. Regular reflection

We will study the domain of validity of regular reflection. First, let us concentrate on the steady state solution. This is represented in Fig. 14. We have, in the notation of Fig. 8, an unperturbed state with $\sigma_0 = \eta_0 = 0$, an incoming shock with parameters $\alpha > 0$, $\sigma_1 > 0$, and $\eta_1 = -\alpha\sigma_1$ and a reflected shock with $\sigma = \sigma_2$ and inclination β that restores η to zero. Entropy requires that $\sigma_2 > \sigma_1 > 0$.

The incoming shock has horizontal velocity $c = \sigma_1/2 + \alpha^2$, which has to match the reflected $c = (\sigma_1 + \sigma_2)/2 + \beta^2$. This gives the condition

$$\sigma_2/2 + (\beta^2 - \alpha^2) = 0. \quad (13)$$

In addition, the reflected shock has to restore the velocity normal to the wall to zero. Then

$$\beta(\sigma_2 - \sigma_1) + \alpha\sigma_1 = 0. \quad (14)$$

From (13) and (14),

$$(\beta - \alpha)(2\beta(\beta + \alpha) + \sigma_1) = 0$$

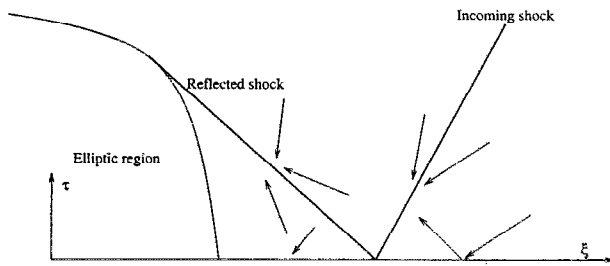


FIG. 15. Characteristics in unsteady regular reflection. The incident and reflected shocks belong to different families of characteristics. All spatial and temporal nonuniformities are confined to the elliptic domain.

so either $\beta = \alpha$, $\sigma_2 = 0$ (a nonentropic reflected shock which completely cancels out the incoming one), or

$$\beta = (-1/2 \pm 1/2 \sqrt{1 - 2\sigma_1/\alpha^2})\alpha \quad (15)$$

with corresponding

$$\sigma_2 = (1 + \sigma_1/\alpha^2 \pm \sqrt{1 - 2\sigma_1/\alpha^2})\alpha^2. \quad (16)$$

These solutions break for $\sigma_1/\alpha^2 > 1/2$; hence no regular reflection can occur beyond this limit. When regular reflection is allowed, there are two possible solutions, both satisfying the entropy condition. The choice of one or the other must arise from considerations involving causality; it is in principle conceivable that different initial conditions could give rise to the two solutions. In order to elucidate which occurs in our problem, we need therefore to study the unsteady case.

The initial condition corresponding to the time at which the incident shock hits the wedge has already been plotted in Fig. 8. As both the asymptotic equations and the initial and boundary conditions are invariant under the stretching (6) the solution must be a function of $\xi = x/t$ and $\tau = y/t$ alone, so Eqs. (7) apply.

The two families of characteristics (8) are plotted in Fig. 15 in the different regions of an unsteady regular reflection. The incoming shock belongs to the family of characteristics approaching the wall, while the reflected shock must belong to the family getting away from it. The elliptic domain of (7), also plotted in Fig. 15, completes the picture of regular reflection; it is the region where the steady pattern has not yet arisen.

We can verify, at least partially, that the configuration of Fig. 15 is correct, by solving the linear problem exactly with the techniques of Sec. III D. In the linear case, (15) and (16) give $\beta = -\alpha$ and $\sigma_2 = 2\sigma_1$, which, together with $\eta_1 = -\alpha\sigma_1$, yield the picture of Fig. 16. Now, if we recall that $S = -\tau/2 + \sqrt{\tau^2/4 + \xi}$, we have to build an analytic function $G(S)$ with the boundary conditions of Fig. 17. The solution is

$$G(S) = -\frac{\alpha\sigma_1}{\pi} \log((\alpha + S)(\alpha - S))$$

so

$$F(S) = \int \frac{-G'(S)}{S} dS = \sigma_1 \left[2i - \frac{1}{\pi} \log\left(\frac{\alpha + S}{\alpha - S}\right) \right].$$

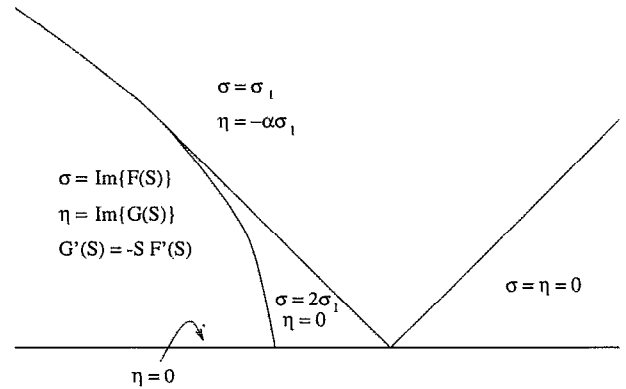


FIG. 16. Linear regular reflection. The discontinuity in the data along the parabolic line will give rise to a fan-like singularity in the elliptic domain, centered at the point where the reflected wave meets the parabolic line.

Then $\sigma(\xi, \tau)$ and $\eta(\xi, \tau)$ inside the elliptic domain are given by

$$\begin{aligned} \sigma &= \sigma_1 \left[2 - \frac{1}{\pi} \tan^{-1} \left(\frac{2\alpha \sqrt{|\tau^2/4 + \xi|}}{\alpha^2 + \xi} \right) \right], \\ \eta &= -\frac{\alpha\sigma_1}{\pi} \tan^{-1} \left(\frac{\tau \sqrt{|\tau^2/4 + \xi|}}{\alpha^2 - \xi - \tau^2/2} \right), \end{aligned} \quad (17)$$

where \tan^{-1} is taken to range from 0 to π . This exact linear solution is plotted in Fig. 18. To show that essentially the same pattern arises in nonlinear regular reflection, we have plotted the numerical solution to a case with $\sigma_1/\alpha^2 = 0.2$ in Fig. 19. In the three-dimensional (3-D) plots, σ is viewed from ahead of the incident shock and $-\eta$ from behind the reflected one.

In the general nonlinear case, the boundary of the elliptic region touches the wall at $\xi = x/t = \sigma_2$. This is the "sonic" point corresponding to σ_2 ; behind it, a constant state with $\sigma = \sigma_2$ cannot sustain itself, since the information from the incoming shock would never reach it. In the pictures drawn so far, we have assumed that this point lies behind that at which the incident shock meets the wall. Let us now elucidate under which conditions this is the case.

At the wall, the incoming shock has $\xi_{\text{inc}} = \sigma_1/2 + \alpha^2$. On the other hand, from (16), the sonic point corresponding to σ_2 is

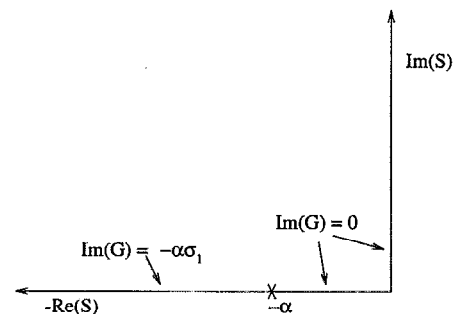


FIG. 17. Boundary conditions for $G(S)$.

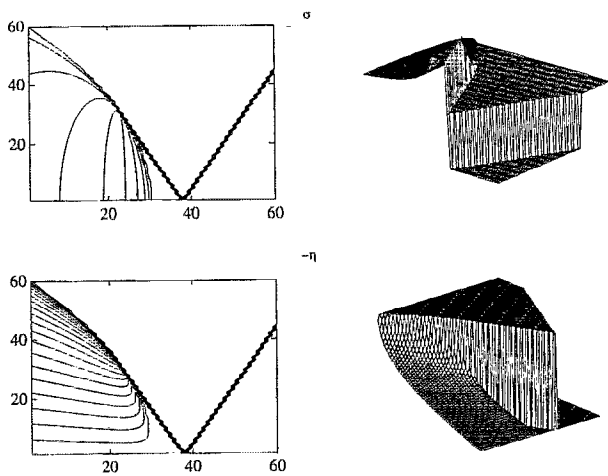


FIG. 18. Linear regular reflection (exact solution). The fan-like singularity at the junction of the reflected wave and the parabolic boundary has the structure of a linear singular ray.

$$\xi_{\text{son}} = \alpha^2 + \sigma_1 \pm \sqrt{\alpha^2 - 2\sigma_1}. \quad (18)$$

From this we can already see that, in order to have $\xi_{\text{son}} < \xi_{\text{inc}}$, we need to adopt the minus sign in (15) and (16). This corresponds to choosing the solution with smaller σ_2 and more oblique reflected pattern. Furthermore, a small computation shows that $\xi_{\text{son}} < \xi_{\text{inc}}$ also implies that

$$\sigma_1/\alpha^2 < \frac{1}{(1 + \sqrt{5}/2)} = 0.4721 < 0.5. \quad (19)$$

A more conceptual reason why the minus sign has to be chosen in (15) is that, in the solution with the plus sign, the constant state behind the “reflected” shock arises from the conditions at ∞ , not from information reflected from the wall. In the language of Fig. 15, both the incident and

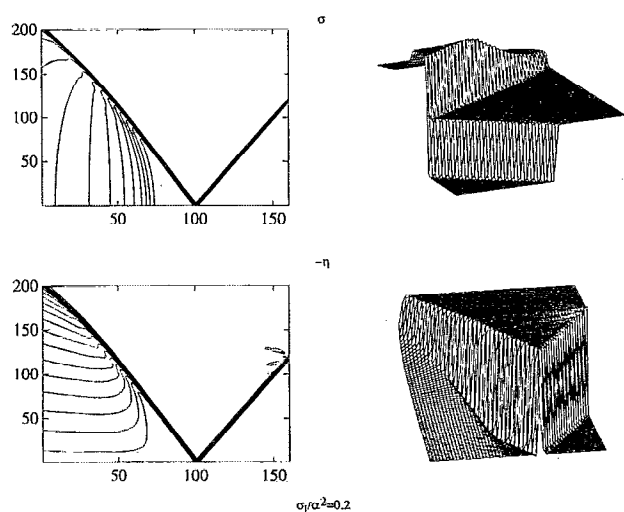


FIG. 19. Nonlinear regular reflection (numerical). The fan-like singularity is “eaten” by the reflected shock wave, which moves more slowly than the singular point.

“reflected” shock belong to the family of characteristics approaching the wall. It is clear that such solutions would be highly artificial, and that it is improper to call the second shock “reflected” in this context. A truer interpretation is that we have two incident shocks, arranged just right so that their reflections cancel.

So far, we know the following about the range of validity of regular reflection for the asymptotic equations: A locally steady solution with a regularly reflected shock can only be obtained, for the wedge problem, when $\sigma_1/\alpha^2 < 0.4721$. However, a solution with a reflected shock arising from the wall is in principle plausible up to $\sigma_1/\alpha^2 = 0.5$. If a “regular” reflection occurs between $\sigma_1/\alpha^2 = 0.4721$ and 0.5, the state behind the reflected shock will be nowhere uniform. For $\sigma_1/\alpha^2 > 0.5$, neither regular reflection nor a standard Mach stem are allowed, as the following subsection shows.

B. The asymptotic equations do not admit triple shocks

We show here that Eqs. (1) do not admit triple shocks separating regions where the solution is continuous. Notice that such triple-shock configuration is not possible for the original equations of gas dynamics either. In that context, the occurrence of slip-lines gives one extra degree of freedom which, in many cases, accounts for the appearance of triple shocks. As the shocks become weaker and more parallel, however, the changes of entropy, which are of higher order, become negligible, and the slip lines are so weak that they no longer suffice to make triple shocks permissible. In the context of Eqs. (1), this manifests itself in the complete absence of vorticity—and therefore of slip lines. The following argument shows that, unless some different kind of discontinuity appears, triple shocks in this regime cannot arise.

We need to characterize the family of shocks having one common (moving) point. This point we can take to be given by $x = ut$, $y = vt$. The jump conditions (3) imply that, for a shock with inclination specified by its cotangent α ,

$$\bar{\sigma} = u - \alpha v - \alpha^2, \quad (20)$$

where $\bar{\sigma}$ is the average of σ on the two sides of the shocks.

Let us now consider three shocks, with a common point that moves at velocity (u, v) , separating three regions where, for simplicity, we will assume σ and η to be constant (see the note at the end of the proof). As shown in Fig. 20, we will denote the three regions with Roman numbers I, II, and III, while the shocks will be identified with Arabic numbers, 1 for the shock separating the regions II and III, 2 for the one between regions I and III, and 3 for that between regions I and II. We will call α_i the cotangent of the angle θ_i .

The jumps in σ across the shocks and the averages of σ on both sides of them are connected by the following relations:

$$(\sigma_{\text{III}} - \sigma_{\text{II}}) = 2(\bar{\sigma}_2 - \bar{\sigma}_3),$$

$$(\sigma_{\text{I}} - \sigma_{\text{III}}) = 2(\bar{\sigma}_3 - \bar{\sigma}_1),$$

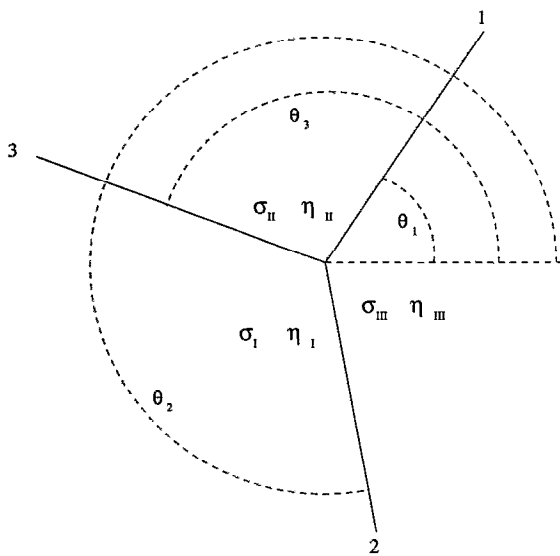


FIG. 20. Triple shock configuration. The only crucial assumption is that the solution is continuous inside the three domains separated by the shocks.

$$(\sigma_{II} - \sigma_I) = 2(\bar{\sigma}_1 - \bar{\sigma}_2).$$

Using (20), we can transform these into

$$(\sigma_{III} - \sigma_{II}) = 2v(\alpha_3 - \alpha_2) + 2(\alpha_3^2 - \alpha_2^2),$$

$$(\sigma_I - \sigma_{III}) = 2v(\alpha_1 - \alpha_3) + 2(\alpha_1^2 - \alpha_3^2),$$

$$(\sigma_{II} - \sigma_I) = 2v(\alpha_2 - \alpha_1) + 2(\alpha_2^2 - \alpha_1^2).$$

We can get the jumps in η from the jump conditions $[\eta] = \alpha[\sigma]$:

$$(\eta_{III} - \eta_{II}) = \alpha_1(2v(\alpha_3 - \alpha_2) + 2(\alpha_3^2 - \alpha_2^2)),$$

$$(\eta_I - \eta_{III}) = \alpha_2(2v(\alpha_1 - \alpha_3) + 2(\alpha_1^2 - \alpha_3^2)),$$

$$(\eta_{II} - \eta_I) = \alpha_3(2v(\alpha_2 - \alpha_1) + 2(\alpha_2^2 - \alpha_1^2)).$$

Adding these up, we obtain the consistency requirement

$$0 = \frac{1}{2} \sum_{i=1}^3 [\eta]_i = \alpha_1(\alpha_3^2 - \alpha_2^2) + \alpha_2(\alpha_1^2 - \alpha_3^2) + \alpha_3(\alpha_2^2 - \alpha_1^2).$$

Now think of this as an equation for α_1 , with α_2 and α_3 fixed. It clearly has the roots $\alpha_1 = \alpha_2$ and $\alpha_1 = 3$. It can have no more, because the equation is quadratic. But these two roots are trivial; they yield a configuration that reduces to a single shock. Hence triple shocks are not allowed, as was to be proved.

Note: Although for simplicity we have worked with straight shocks separating constant states, the theorem remains valid under more general conditions. It is enough to assume that each shock has a definite tangent as it approaches the triple shock, and that both σ and η are continuous at the triple point inside each of the three regions into which the shocks divide the plane.

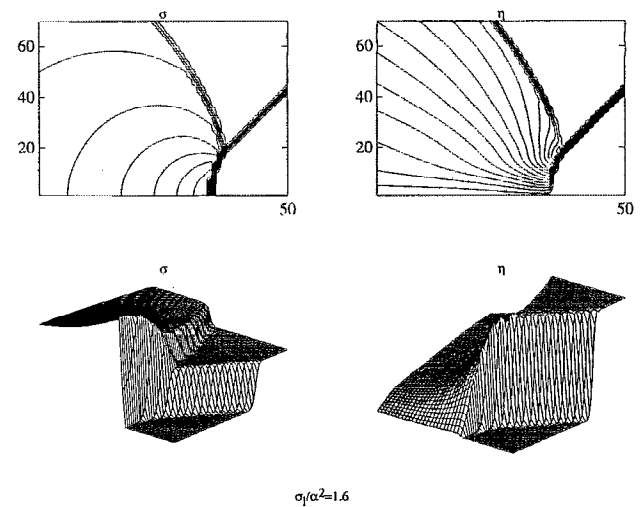


FIG. 21. Pseudo-Mach-stem, exhibiting a triple point and a strongly non-uniform region behind the reflected wave.

C. Irregular reflection

What happens when regular reflection is no longer allowed? To get a first glimpse of the answer to this question, we have plotted in Fig. 21 the numerical solution to Eqs. (1) with $\sigma_1/\alpha^2 = 1.6$, well inside the domain of irregular reflection. A clear triple point appears, with three waves which do look like shocks. We need more solid evidence for this, since it seems to contradict the theorem of the previous section. It has in fact been argued (see Refs. 10, 12, and 13) that there is no reflected shock in this regime; that the incident shock merely bends until becoming parallel to the wall and behind this shock only a smooth compression wave forms. We will show that this is unlikely by relating the question of smoothness to that of the location of the elliptic and hyperbolic domains. But first we can perform some simple tests.

It is hard to distinguish visually between a shock and a very steep compression wave. However, in a numerical computation, the width of a shock should scale with the grid size (typically two meshpoints for a strong shock and five or more for very weak ones for second order Godunov-like schemes), while every contour line of a smooth wave, once resolved, should be basically invariant under further refinements. Therefore a good check for shocks is the behavior under grid refinements. If we could refine our grid forever, this test would always yield a definite answer. As we are bounded by our computing capabilities, however, we can only say the following: if for our finest grid the wave's width, measured as the distance between the contour lines of two fixed values, keeps scaling with the grid size, we are either in the presence of a discontinuity, or we have a wave so steep that even so fine a grid cannot tell it from a discontinuity. If the two values are very far apart and the finest grid is really very fine, common sense will tell us that a shock is a lot more likely. In Fig. 22 we have plotted details of the solution to a fixed problem with two grids, one five times finer than the other in each direction.

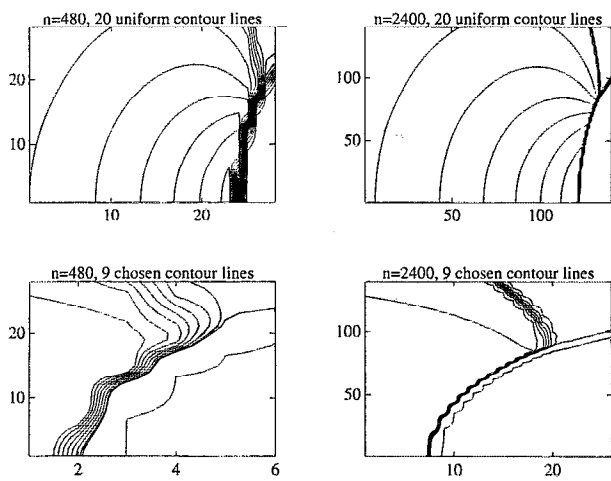


FIG. 22. Contour lines of σ for two computations over the same domain and data, with grid sizes scaled by a factor of 5. The reflected wave has a finite jump across a band of about one grid size; this strongly indicates the presence of a discontinuity.

The number n in the figure is a measure of the grid size, which will be defined in Sec. IV. For this problem, $\sigma_0 = -0.8$, $\sigma_1 = -0.4$, and $\alpha = 0.5$, so $(\sigma_1 - \sigma_0)/\alpha^2 = 1.6$. The numbers labeling the axis of the plots represent mesh points. In the two top figures, we have plotted a relatively distant view, to show that both grids resolve the field away from the shocks consistently. In the plots at the bottom, we have made a more extreme close-up of the triple point in the x -direction, to be able to appreciate the exact width of the waves. The contour lines in these plots were chosen, from right to left, at the values -0.79 (to mark the front edge of the incident shock), -0.41 and -0.39 (to trace the back edge of the incident shock and the front edge of the reflected wave), -0.35 , -0.3 , -0.25 , -0.2 , -0.15 , and -0.1 . Looking first at the incident shock, we observe that it has a width of about one grid size in both resolutions. Turning next our attention to the reflected wave, we see that the interval between -0.39 and -0.2 also scales consistently with the grid size; it has actually a width of only one grid size as well. The value $\sigma = -0.15$ probably lies close to the back edge of the reflected shock, while $\sigma = -0.1$ is resolved by both computations as being away from the leading edge of the wave. The similarity of the two computations is striking; the fact that the predicted shock has a jump of about 0.2, i.e., half the intensity of the incident shock, resolved in just one cell with $\Delta x = 0.01$, seems to us compelling evidence that the reflected wave is indeed a shock. We will now show more subtle arguments to the same effect.

Recall that Eqs. (7) switch from hyperbolic to elliptic when $\tau^2 + 4\xi - \sigma$ becomes negative. We can compute this expression at every point in the numerical solution, and thus determine the solution's local character. The boundary between the two domains is shown with continuous solid trace in Fig. 23, with the (dotted) contour lines of σ as background. We see that this boundary coincides with the reflected front. Then the hyperbolic domain consists

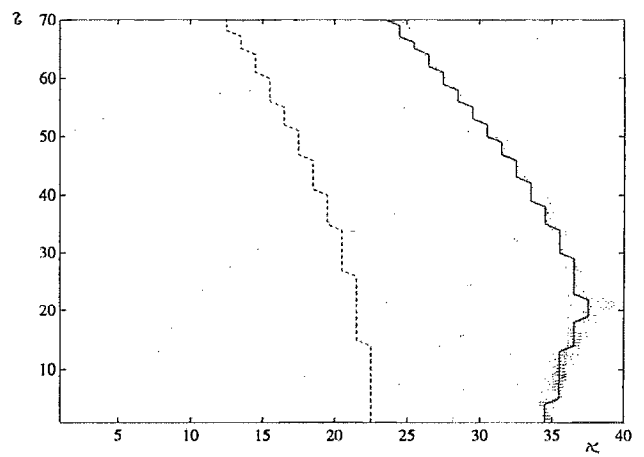


FIG. 23. Real and hypothetical boundaries of ellipticity. The solid line marks the real (numeric) boundary; the dotted line corresponds to the parabolic line computed with $\sigma = \sigma_1$. If the reflected wave were not a shock, both lines should coincide.

solely of constant states separated by the incident shock, while all nonuniformities in space and time are confined to the elliptic domain. There is another line marked on Fig. 23 with dashes: it corresponds to a hypothetical boundary of ellipticity computed with $\sigma = \sigma_1$. This should coincide with the previous one were the reflected front not a shock, because then the value of σ at the head of the reflected wave would be σ_1 by continuity. We conclude that this cannot be the case, since the distance between the two lines exceeds by far the order of magnitude of any possible numerical error.

This argument was based on numerical evidence. Many of its components, however, can be sustained on purely analytic grounds. We will take $\sigma_0 = 0$ and consider the range $\sigma_1/\alpha^2 < 2$. As regular reflection cannot take place for $\sigma_1/\alpha^2 > 1/2$, this range covers the transition between regular and irregular reflection. We will show that, under one assumption, a smooth reflected wave cannot hold in this range. Recall that the location of the incident shock is given by

$$\xi = \frac{\sigma_1}{2} + \alpha^2 + \alpha\tau$$

while the condition for ellipticity, for a state with $\sigma = \sigma_1$, is

$$\xi < \sigma_1 - \frac{\tau^2}{4}.$$

As $\tau > 0$ and $\alpha^2 > \sigma_1/2$ by hypothesis, we see that, if there is a smooth reflection wave, its leading edge will have $\sigma = \sigma_1$, and will therefore lie inside the hyperbolic domain of Eqs. (7), at least in some neighborhood of the triple point. Then the reflected wave must lie on a characteristic of the equations. To which of the two families of characteristics may it belong? In our chosen range of parameters, the characteristics of the same family of the incident shock have positive slope, i.e., $d\xi/d\tau > 0$. But in all the experimental and numerical results known to us, including those used in Refs. 10 and 12 to support the theory of the

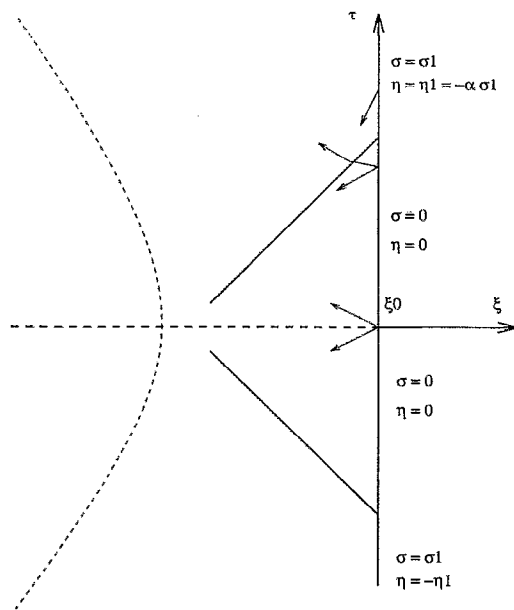


FIG. 24. Initial value problem which shows that a smooth reflected wave cannot arise. The dotted line marks the location of the parabolic line, boundary of the elliptic domain, computed with $\sigma = \sigma_1$. For the assumed range of parameters, this line lies entirely behind the point where the incident shock wave, if continued, would hit the wall.

“smooth compression wave,” the reflected wave has negative slope. We conclude that the assumed smooth reflected wave must belong to the other family of characteristics, those emanating from the wall, as is the case in regular reflection. This assumption, which can also be justified invoking causality, is equivalent to the statement that $-\xi$ is a time-like variable for $\xi > \xi_0$, for some ξ_0 which is strictly smaller than the value of ξ at the triple point. The necessity of this assumption on the family of characteristics to which a smooth reflected wave must belong is the only reason why we cannot yet call our argument against the existence of such wave a theorem. Once this is assumed, however, a contradiction follows immediately.

Consider the initial value problem plotted in Fig. 24, where $-\xi$ plays the role of time. For simplicity, we have replaced the wall by an axis of symmetry, in order to give initial data on the whole $\xi = \xi_0$ axis, where ξ_0 must be chosen large enough to lie ahead of the reflected wave. This initial value problem clearly has a solution consisting of the incident shock and its mirror image, up to the time when they meet at the wall. But this solution is unique. Uniqueness of the solution to homogeneous hyperbolic systems was proved by Diperna in Ref. 24; the extension to the case with variable coefficients should be straightforward, particularly for 2×2 systems in one space dimension. Therefore the assumption of existence of another solution with a smooth reflected wave cannot hold, as we wanted to prove. To invalidate the uniqueness argument, we need $-\xi$ not to be a valid time at the triple point, and this forces the reflected wave to be a shock, since $-\xi$ is time-like along the incident shock all the way to the wall for $\sigma = \sigma_1$.

We have therefore shown that, despite the theorem of

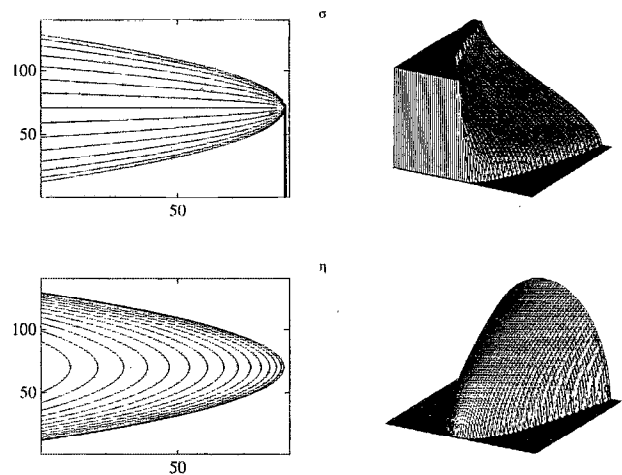


FIG. 25. Linear singular ray (exact solution). At the edge of the compressive wave, the solution has vertical slope.

Sec. III B, triple shocks are required in at least some range of irregular reflection. Before attempting a way out of this paradox, we will see, in the following two sections, how it arises in two different contexts: in a type of modified singular ray and in both quasilinear and fully nonlinear focusing.

D. Standard and modified singular rays

At the standard singular ray occurring when a shock reaches the end of an obstacle, the many symmetries of both Eqs. (1) and the initial data of Fig. 9(b) reduce the whole phenomenon to a single, time independent configuration. To see this, observe that, on the one hand, the invariance under stretching (6) makes the solution depend only on x/t and y/t . On the other hand, the Galilean invariance (4) turns the choice of σ_0 arbitrary. Finally, the invariance under the similarity transformation (5) reduces the choice of σ_1 to that of appropriate x/t and y/t scales. Therefore, the result of any experiment at any time and location can be drawn from one single picture!

This reduction of all nonlinear singular rays to one configuration makes the singularity of the linear limit even more striking: there appears to be two—and only two—distinct patterns, one nonlinear—but not amplitude dependent!—and one linear. The latter is a limiting case of the former in two ways: for fixed x , y , and t , as the amplitude goes to zero and, for fixed amplitude, as x/t and y/t go to infinity with y^2/x fixed.

With the same methodology of Sec. IV A we can compute the exact solution in the linear case. The solution is

$$\begin{aligned} \sigma &= \frac{2}{\pi} \tan^{-1} \left(\frac{-\tau}{\sqrt{-(\tau^2 + 4\xi)}} \right), \\ \eta &= \frac{1}{\pi} \sqrt{-(\tau^2 + 4\xi)}, \end{aligned} \quad (21)$$

plotted in Fig. 25. Next we consider the nonlinear case. From the discussion above, the choice of parameters here

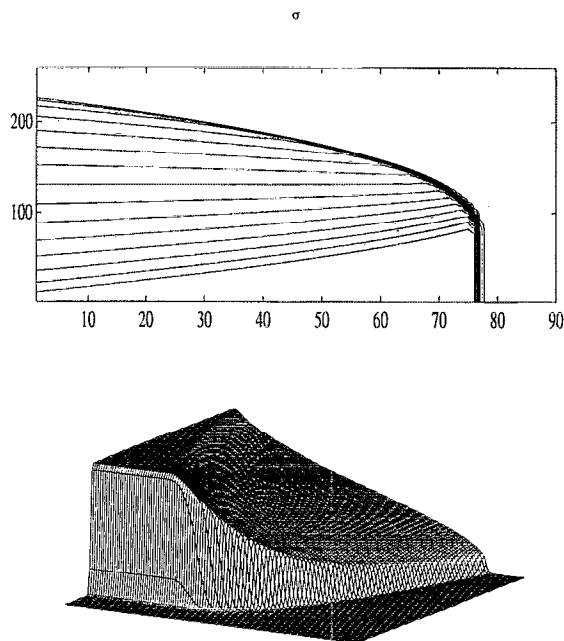


FIG. 26. Nonlinear singular ray (numerical). The compressive wave is now a shock, and the fan-like singularity has disappeared.

is a question of convenience alone. We have adopted $\sigma_1=1$, $\sigma_0=0$ [see Fig. 9(b)]; the numerical results at $t=2$ are plotted in Figs. 26 and 27. As we can see, the nonlinear structure resembles a lot the linear one, with two important differences: the singularity that appears in the elliptic region of the linear solution at $\xi=\tau=0$ is “eaten” by the shock, that moves backward relative to the sound velocity behind it, and the infinite slope at the end of the compressive

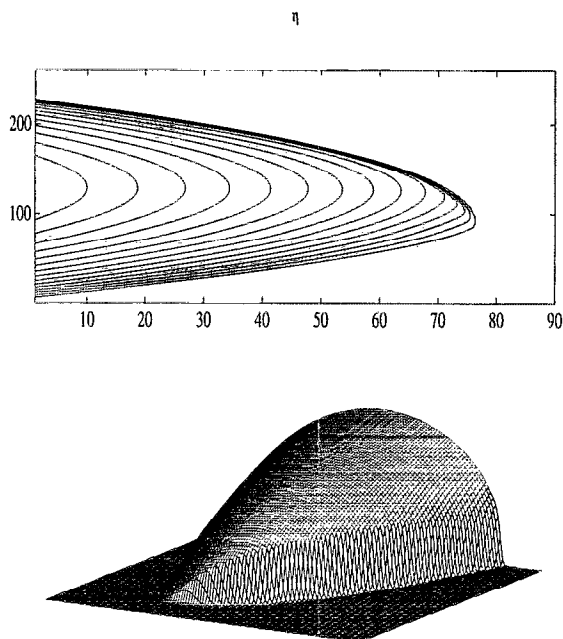


FIG. 27. Nonlinear singular ray (numerical). Notice the shock slicing the otherwise smooth solution.

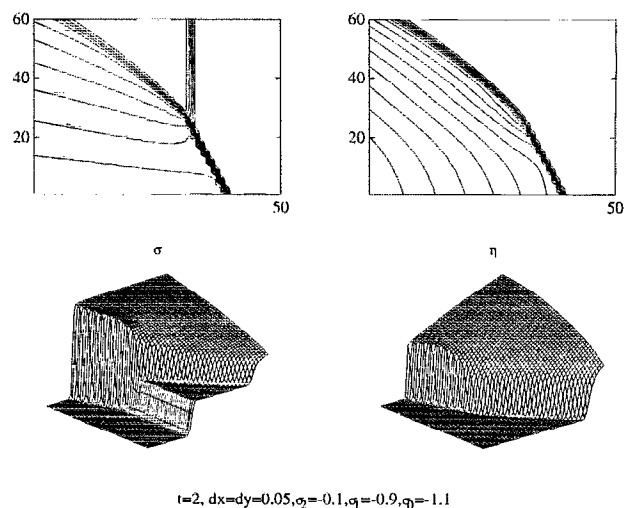


FIG. 28. Singular ray with triple shock (detail). The von Neumann paradox arises here in a conceptually simpler context.

sive wave (the square-root singularity at the edge of the linear elliptic region) breaks into a shock. This last point, that will be shown below to be somewhat paradoxical, can be “proved” by the same technique of Fig. 23, by looking at the location of the boundary between elliptic and hyperbolic domains. However, in this case the same idea can be made into a purely analytic proof.³

As we have seen, nonlinear singular rays have a relatively simple structure, much easier to explain, qualitatively at least, than pseudo-Mach-stems, arêtes, and caustics. It would be interesting, therefore, to make up some intermediate object that, sharing the basic behavior of singular rays, incorporates some of the paradoxes related to triple points. Such an object is readily available in the initial configuration of Fig. 9(c). If we let this configuration progress in time (see Fig. 28, where we have taken, in the notation of Fig. 9, $\sigma_0=-0.1$, $\sigma_1=0.9$, and $\sigma_2=1.1$), the shock between states 0 and 2 will move forward faster than that between 0 and 1, since $\sigma_2 > \sigma_1$. The latter will, therefore, intersect the compressive front of this modified singular ray. If this is still a shock, as it is when $\sigma_1=\sigma_2$, we will have again a triple shock intersection in principle forbidden by the theorem of Sec. IV B. But we can prove that, for a range of parameters, this triple shock has to arise.³ This fact enables us to state the von Neumann paradox in a way that does not depend on delicate experimental measurements: If there is a solution to Eqs. (1) with the initial data of Fig. 9(c), it needs to develop triple shocks. On the other hand, triple shocks separating smooth states are not allowed by the equations.

E. Weak and strong focusing of shocks

We will illustrate the two possible configurations, quasilinear and fully nonlinear, with two typical runs. In the first one (Figs. 29–31), we see the initial flattening, delayed focusing and eventual folding of a relatively weak shock wave. In the notation of Fig. 10, we have $\sigma_0=0$, $\sigma_1=0.1$,

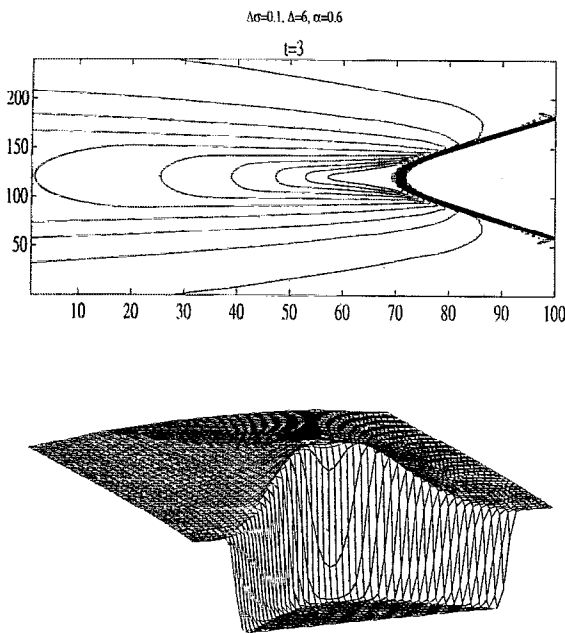


FIG. 29. Quasilinear focusing. Initial flattening of the front.

$\Delta=6$, and $\alpha=0.6$. In the second (Figs. 32 and 33), a stronger wave with $\sigma_0=0$, $\sigma_1=0.5$ and the same geometric parameters is shown as it goes through front flattening, formation of compressive diffraction waves and appearance of diverging triple shocks. The parameter that will determine whether the front will eventually fold on itself or flatten up, namely the quotient $(\sigma_1 - \sigma_0)/\alpha^2$, takes in the two cases the values 0.28 and 1.39, corresponding to regular and irregular reflection respectively.

In Fig. 29, we see the initial nonlinear flattening of a weak focusing shock. The time in Fig. 30 corresponds

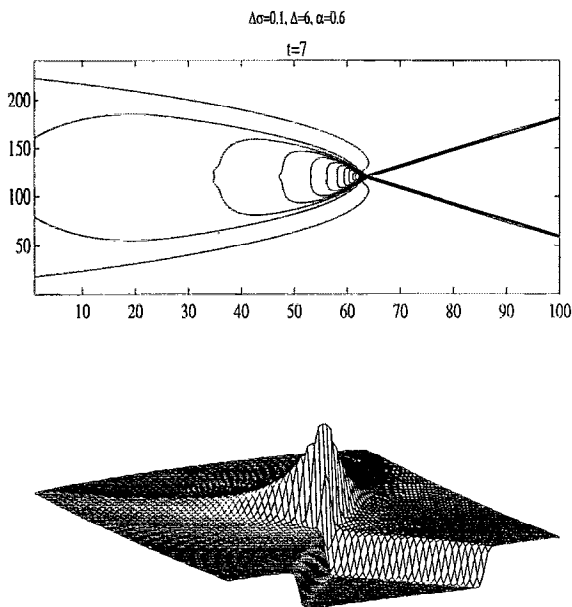


FIG. 30. Quasilinear focusing. Collision of the two triple points.

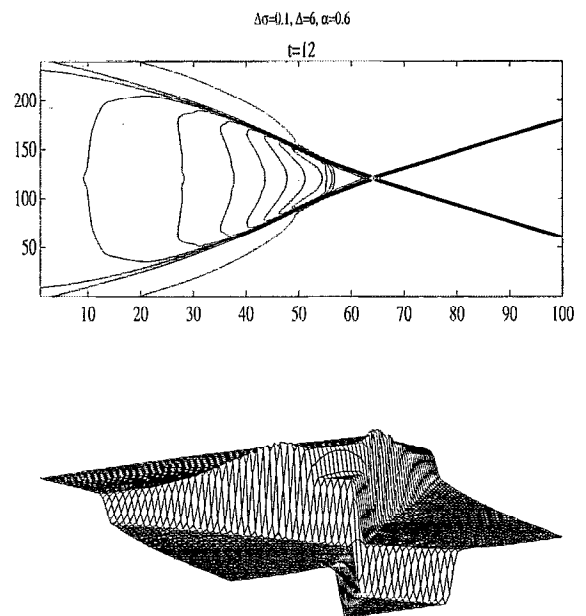


FIG. 31. Quasilinear focusing. Swallow-tail with triple shocks.

roughly to that of a linear arête (or rather a perfect focus, since the parabolic initial front adopted here corresponds to a circle in the original equations). In Fig. 31, we see the nonlinear equivalent of the linear "swallow-tail." There is an important difference between quasilinear focusing and regular reflection, in that the former has a triple-shock encounter where the latter has a singular ray. This can be seen in Fig. 31, where the inverted front at the end of the uniform pressurized region is a compressive shock. This contrasts with the smooth expansion that arises in the same place in regular reflection (see Fig. 18). To clarify this, we have plotted in Fig. 34 a schematic cut at $y=0$ of Figs. 18 and 31. We observe in Fig. 31 an inverted pseudo-Machstem where in the linear case we should find a caustic. This

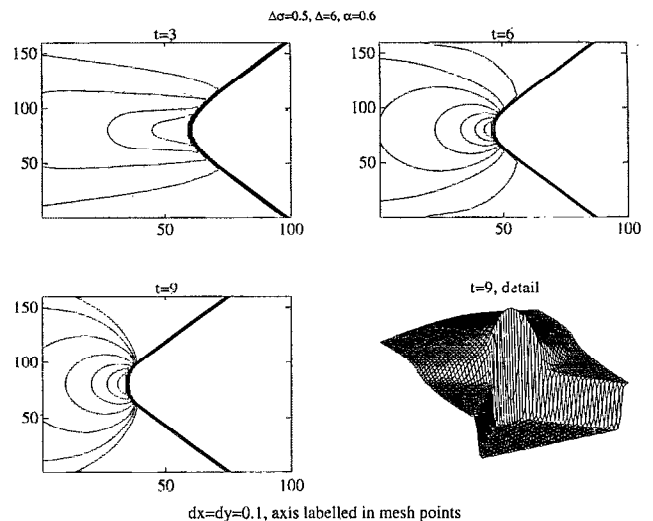


FIG. 32. Fully nonlinear focusing. Initial flattening of the front.

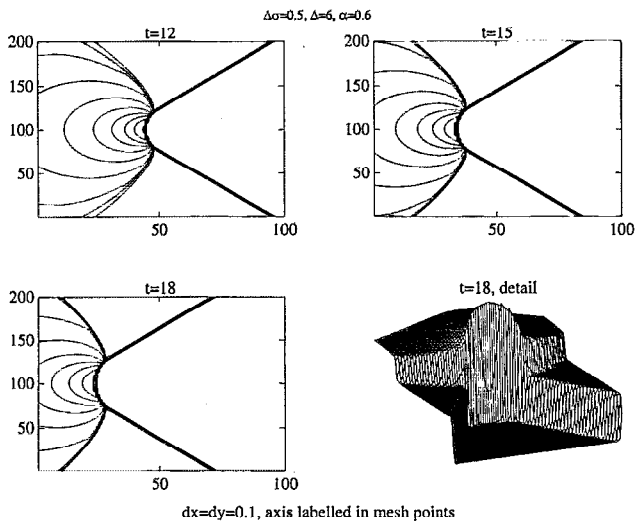


FIG. 33. Fully nonlinear focusing. The diffracted compressive waves have developed into shocks, yielding a new instance of the von Neumann paradox.

provides a new tool for analyzing triple shocks, namely a linear limit. We did not have this in irregular reflection, since this was inherently nonlinear: before the amplitude vanished, we had to switch to regular reflection, thus losing the triple point altogether.

Figure 32 shows the flattening of a stronger concave shock, and the formation of diffracted compression waves behind it. In Fig. 33, these waves have steepened into shocks, giving rise to triple points, completely analogous in this case to those of irregular reflection. Therefore the numerics agree with the experimental results of Sturtevant and Kulkarny and the theoretical predictions of Sec. III. We conclude that Eqs. (1) do capture the transition between linear and nonlinear focusing, and that a complete understanding of both the quasilinear and weakly nonlinear regimes must await the resolution of the von Neumann paradox.

V. SINGULAR BEHAVIOR BEHIND TRIPLE SHOCKS

We have proved in Sec. IV B that Eqs. (1) do not admit triple shocks dividing regions where the variables vary continuously. But triple shocks do arise in a variety of

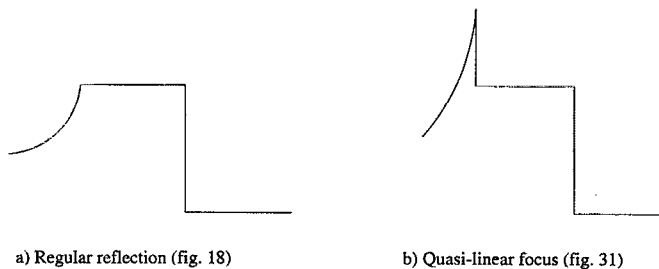


FIG. 34. Sections at the wall and axis of symmetry of a regular reflection and a quasilinear focus. The latter has a shock followed by a rarefaction where the former has only a rarefaction.

situations. The conclusion we can draw is that the states separated by these shocks are not all smooth. As two of these states are constant, all singularities must lie in the nonuniform region behind the triple point, where Eqs. (7) are elliptic. This imposes a serious constraint on the class of admissible singularities. In particular, fan-like singularities are not allowed, as the following argument shows: Let us denote the singular point by (ξ^*, τ^*) and the variable associated with the fan by $S(\xi, \tau)$. Unless another variable with unbounded derivatives plays a role in the solution, a dominant balance in the neighborhood of (ξ^*, τ^*) yields the equations

$$((-\xi^* + \sigma)S_\xi - \tau^* S_\tau) \sigma'(S) + S_\tau \eta'(S) = 0,$$

$$S_\tau \sigma'(S) - S_\xi \eta'(S) = 0,$$

which only have nontrivial solutions if

$$S_\tau / S_\xi = \tau^* / 2 \pm \sqrt{\tau^{*2} / 4 + \xi^* - \sigma}.$$

For this to be real, the point (ξ^*, τ^*) must lie in the hyperbolic domain, which we know cannot be true.

This same argument holds in the linear case. In the latter, however, the definition of hyperbolic and elliptic domains does not depend on σ . This allows us to take the point (ξ^*, τ^*) on the boundary between the two domains, which yields the singularities we have already found for linear singular rays. This is not possible in the nonlinear case, where the condition of (ξ^*, τ^*) lying on the sonic line can only be achieved for one value of σ , not the required whole interval [the hypothesis that only η be multivalued at the triple point cannot hold, since then no term could balance the unbounded derivatives of η in (7)]. Therefore, there must be another singular variable R , different from S , that behaves in such a way as to contribute to the dominant balance at the triple point. But it is easy to see, on purely geometrical grounds, that such second variable cannot be bounded. As σ cannot conceivably go to infinity, since it represents the speed of sound, the unbounded variable has to be η . Moreover, η cannot go to infinity along all paths reaching (ξ^*, τ^*) . In particular, it cannot do so along the shocks, since otherwise these would have to be horizontal, something impossible to achieve with finite σ 's. The only possibility apparently left is that η tend to infinity and σ have a fan-like singularity inside a finite wedge.

In the runs of Sec. IV, however, we never saw any hint of η being unbounded at the triple point. This might be due to the local character of the singularity, which only manifests itself as we approach the triple point along a restricted set of paths. This might make the peak of η very sensitive to numerical viscosity. We will now show that this is indeed the case by conducting a series of new experiments with much finer grids.

The invariance of Eqs. (1) under the stretching (6) yields two equivalent ways of refining a grid: either take smaller Δx , Δy , and Δt 's or compute the solution for longer times. We have randomly used both approaches in the experiments that follow; so we will define, as a measure of the refinement, the number $n = t / \Delta t$. The mesh size of the spatial variables is always $\Delta x = \Delta y = 4 \Delta t$, which satisfies the

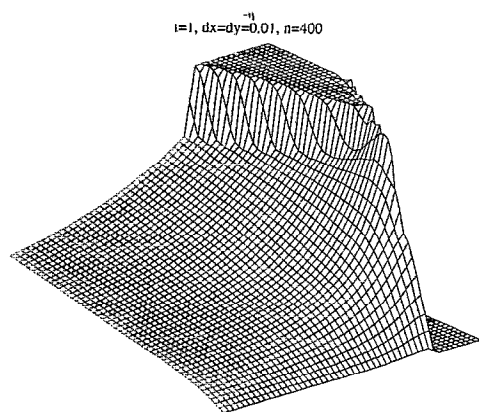


FIG. 35. Singularity not yet visible. Elsewhere the solution is fully resolved.

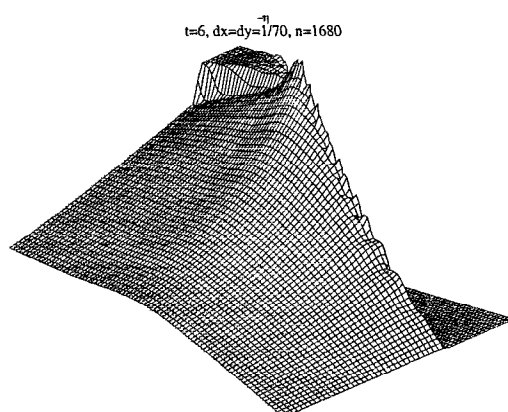


FIG. 37. The singularity becomes more apparent.

Courant–Friederichs condition for the range of σ 's covered. In Figs. 35–38, we see plots of η from a series of experiments on irregular reflection ($\Delta\sigma=0.4$, $\alpha=0.5$) with increasing values of n . The singularity in η , initially hidden by numerical viscosity, gradually manifests itself as the grid is refined. The variable σ , instead, remains basically unchanged and seemingly regular, with at most a fan-like singularity, as can be observed in Figs. 21 and 22.

We have been looking for the analytic structure of this singularity, with some degree of success: we can build families of exact solutions to Eqs. (7) where σ has fan-like singularities and η grows logarithmically inside the elliptic domain. However, we could not yet match these solutions with the jump conditions at the shocks.

VI. CONCLUSIONS

We have shown that a variety of important phenomena involving interactions of weak shock waves at small angles are intimately connected. These include the transition between regular and irregular reflection on rigid walls, the focusing of curved fronts in both the quasilinear and fully nonlinear regimes, and the diffraction patterns at singular rays. Furthermore, all these phenomena can be studied

with a single canonical set of asymptotic equations, those of unsteady small disturbance transonic flow. We have verified both theoretically and numerically that these equations contain all the sometimes paradoxical behavior of the physical situations.

One particular pattern plays a crucial role in these phenomena: the intersection of three shocks, with a very distinctive kind of singularity between two of them. We have shown that these shock intersections do take place and that a singularity is necessary to make them consistent. We have also ruled out a whole class of relatively simple “fan-like” singularities, since these are by nature supersonic, while the region behind a triple point is always subsonic. The only remaining way out of the “triple shock paradox” turns out to be a very localized singularity arising inside a wedge, where one of the the expansion's variables becomes unbounded. A thorough study of this singularity and its consequences for the original equations of gas dynamics will be the subject of further work.

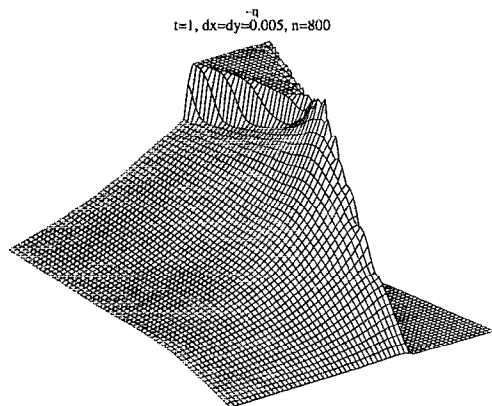


FIG. 36. First glimpse of the singularity.

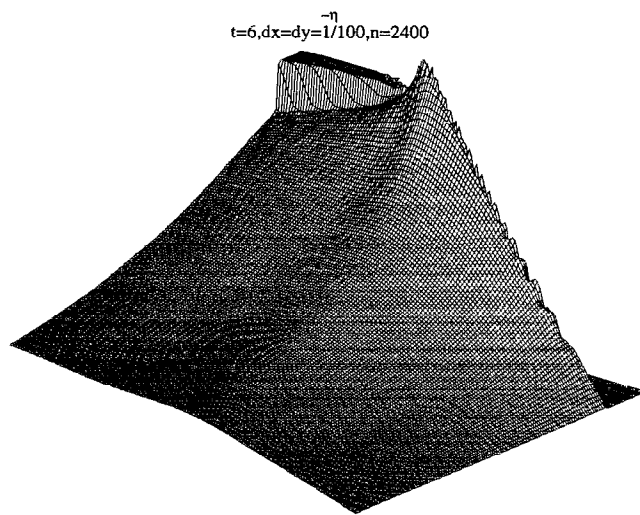


FIG. 38. Finest grid. Further numerical resolution of this singularity requires numerical capabilities beyond our reach at the time of this work.

ACKNOWLEDGMENTS

We would like to thank C. Morawetz and A. Majda for helpful discussions. Partial support for E. G. Tabak was provided by an Alfred Sloan Doctoral Dissertation Award, by NSF under Grant Nos. DMS-9008520 and DMS-9001805 and by DARPA Grant No. N0014-92-J-1796, and for R. R. Rosales by NSF Grant No. DMS-9008520.

- ¹E. G. Tabak, Ph.D. thesis, MIT, Department of Mathematics, 1992.
- ²E. G. Tabak and R. R. Rosales, "A conservative scheme for the numerical solution of the unsteady transonic flow equations," in preparation.
- ³E. G. Tabak and R. R. Rosales, "A simple model for the von Neumann paradox," in preparation.
- ⁴R. R. Rosales and E. G. Tabak, "Interaction of weak shock waves," in preparation.
- ⁵R. N. Buchal and J. B. Keller, "Boundary layer problems in diffraction theory," *Comm. Pure Appl. Math.* **XIII**, 85 (1960).
- ⁶D. Ludwig, "Uniform asymptotic expansions at a caustic," *Comm. Pure Appl. Math.* **XIX**, 215 (1966).
- ⁷B. Sturtevant and V. A. Kulkarny, "The focusing of weak shock waves," *J. Fluid. Mech.* **73**, 651 (1976).
- ⁸J. von Neumann, "Oblique reflection of shocks," in *Collected Works* (Pergamon, New York, 1963), Vol. VI, pp. 238-299.
- ⁹J. von Neumann, "Refraction, intersection and reflection of shock waves," in *Collected Works* (Pergamon, New York, 1963), Vol. VI, pp. 300-308.
- ¹⁰M. Brio and J. K. Hunter, "Mach reflection for the two dimensional Burgers equation," *Physica D* **60**, 194 (1992).
- ¹¹H. M. Glaz, P. Colella, I. I. Glass, and R. L. Deschambault, "A numerical study of oblique shock-wave reflections with experimental comparisons," *Proc. R. Soc. London Ser. A* **398**, 117 (1985).
- ¹²P. Colella and L. F. Henderson, "The von Neumann paradox for the diffraction of weak shock waves," *J. Fluid Mech.* **213**, 71 (1990).
- ¹³H. Hornung, "Regular and Mach reflection of shock waves," *Annu. Rev. Fluid Mech.* **18**, 33 (1986).
- ¹⁴A. Sasoh, K. Takayama, and T. Saito, "A weak shock wave reflection over wedges," *Shock Waves* **2**, 277 (1992).
- ¹⁵J. K. Hunter, "Nonlinear geometrical optics," *Multidimensional Hyperbolic Problems and Computations*, The IMA Volumes in Mathematics and its Applications, edited by J. Glimm and A. Majda (Springer-Verlag, New York, 1991), Vol. 29, pp. 179-197.
- ¹⁶C. S. Morawetz, "Potential theory for regular and Mach reflection of a shock at a wedge," *Comm. Pure Appl. Math.* **45**, 1 (1993).
- ¹⁷R. R. Rosales, "An introduction to weakly nonlinear geometrical optics," *Multidimensional Hyperbolic Problems and Computations*, The IMA Volumes in Mathematics and its Applications, edited by J. Glimm and A. Majda (Springer-Verlag, New York, 1991), Vol. 29, pp. 281-310.
- ¹⁸R. R. Rosales, "Diffraction effects in weakly nonlinear detonation waves," *Proceedings "Seminaire International sur les Problèmes Hyperboliques de Bordeaux"*, Bordeaux, 1988, Springer Lecture Notes (Springer-Verlag, New York, 1989), pp. 227-239.
- ¹⁹M. S. Cramer and A. R. Seebass, "Focusing of weak shock waves at an arête," *J. Fluid Mech.* **88**, 209 (1978).
- ²⁰J. K. Hunter, "Transverse diffraction of nonlinear waves and singular rays," *SIAM J. Appl. Math.* **48**, 37 (1988).
- ²¹G. B. Whitham, *Linear and Nonlinear Waves* (Wiley, New York, 1974).
- ²²J. K. Hunter and J. B. Keller, "Caustics of nonlinear waves," *Wave Motion* **9**, 429 (1987).
- ²³E. G. Tabak, "A second order Godunov method on arbitrary grids," submitted to *J. Comput. Phys.* (1993).
- ²⁴R. J. Diperna, "Uniqueness of solutions to hyperbolic conservation laws," *Indiana Univ. Math. J.* **28**, 137 (1979).